Hydrol. Earth Syst. Sci. Discuss., 10, 11311–11335, 2013
www.hydrol-earth-syst-sci-discuss.net/10/11311/2013/
doi:10.5194/hessd-10-11311-2013

Hydrology and Earth System Sciences
Discussions

Spatially resolved information on karst conduit flow from in-cave dye-tracing

U. Lauber[1], **W. Ufrecht**[2], **and N. Goldscheider**[1]

[1]Institute of Applied Geosciences, Division of Hydrogeology, Karlsruhe Institute of Technology (KIT), Kaiserstr. 12, 76131 Karlsruhe, Germany
[2]private address: Kaiserstr. 45, 70599 Stuttgart, Germany

Received: 5 August 2013 – Accepted: 14 August 2013 – Published: 5 September 2013

Correspondence to: U. Lauber (ute.bellmann@kit.edu, ute.lauber@kit.edu)

Published by Copernicus Publications on behalf of the European Geosciences Union.

Abstract

Artificial tracers are powerful tools to investigate karst systems. Tracers are commonly injected into sinking streams or dolines, while springs serve as monitoring sites. The obtained flow and transport parameters represent mixed information from the vadose, epiphreatic and phreatic zones, i.e., the aquifer remains a black box. Accessible active caves constitute valuable but underexploited natural laboratories to gain detailed insights into the hydrologic functioning of the aquifer. Two multi-tracer tests in the catchment of a major karst spring (Blautopf, Germany) with injections and monitoring in two associated water caves aimed at obtaining spatially and temporally resolved information on groundwater flow in different compartments of the system. Two tracers were injected in the caves to characterize the hydraulic connections between them and with the spring. Two injections at the land surface, far from the spring, aimed at resolving the aquifer's internal drainage structure. Tracer breakthrough curves were monitored by field fluorimeters in caves and at the spring. Results demonstrate the dendritic drainage structure of the aquifer. It was possible to obtain relevant flow and transport parameters for different sections of this system. The highest mean flow velocities (275 m h^{-1}) were observed in the near-spring epiphreatic section (open-channel flow), while velocities in the phreatic zone (pressurized flow) were one order of magnitude lower. Determined conduit water volumes confirm results of water balances and hydrograph analyses. In conclusion, experiments and monitoring in caves can deliver spatially resolved information on karst aquifer heterogeneity and dynamics that cannot be obtained by traditional investigative methods.

1 Introduction

Groundwater flow and contaminant transport in karst aquifers are difficult to predict, because of the unknown configuration and geometry of the conduit network. However, the sustainable use and protection of karst groundwater resources requires detailed

knowledge of the underground flowpath and spring catchment areas. Therefore, tracer tests are often used to investigate the drainage pattern of karst aquifers. Tracer tests primarily deliver clear information on hydraulic connections, spring catchment areas, transit time distributions and linear flow velocities. Relevant conservative and reactive transport parameters, such as dispersion and retardation can be obtained by quantitative analysis and modeling of tracer breakthrough curves (BTCs) (e.g. Geyer et al., 2007; Massei et al., 2006; Morales et al., 2007; Goldscheider et al., 2008). In most cases, tracers are injected into stream sinks, dolines or other surface karst structures, while springs serve as sampling and monitoring sites. Consequently, all obtained data and parameters represent mixed information from the entire flowpath between the injection and recovery sites, i.e. from the unsaturated (vadose), epiphreatic and phreatic (saturated) zones of the aquifer. However, flow velocities and transport parameters are highly variable between and within these zones.

Experiments and monitoring in caves make it possible to obtain more detailed insights into the internal structure and hydraulic functioning of karst aquifer systems (Goldscheider et al., 2008). Owing to the difficult accessibility of active caves and the high experimental efforts, this approach has not been used very often. In this sense, caves are valuable but underexploited natural laboratories for hydrologic research. Perrin et al. (2007) have quantified the role of tributary mixing in chemical variations at a karst spring by means of detailed monitoring inside a cave system. Meiman et al. (2001) have conducted in-cave dye-tracer tests to delineate sub-basins within the Mammoth Cave aquifer. The hierarchical structure of conduit systems is known from speleological observations (Palmer, 1991) and numerical simulations of speleogenesis (Gabrovsek et al., 2004; Dreybrodt et al., 2010). Tracer tests in caves can help to reveal the drainage structure of inaccessible conduit systems (e.g. Smart, 1988). In-cave tracer tests were also used to determine flow velocities and dispersion in open-channel cave streams at local scales (Hauns et al., 2001) and to compare the transport of solutes and colloids (Göppert and Goldscheider, 2008). Tracer injections at

the land surface and monitoring water inlets in caves can help to quantify water storage, percolation and contaminant transport in the epikarst zone (Pronk et al., 2009).

In order to obtain spatially and temporally resolved information on conduit flow in karst aquifer systems, a karst catchment in South Germany that includes two major caves and is drained by a large spring was selected as test site for this study. More than 65 tracer tests have been conducted in the area since 1927, but all injections were done at the land surface, mostly into dolines or stream sinks (Villinger and Ufrecht, 1989; Selg and Schwarz, 2009). Therefore, the catchment area of the spring is well known (Armbuster and Selg, 2006), while the internal drainage structure of this aquifer system was completely unknown, owing to the extreme difficulties in accessing the caves. Since 2010, a drilled shaft permits access to the larger of the two caves without diving. This paper presents the first tracer tests that were done inside the active conduit network of this karst system. The experimental approach consists of two in-cave dye-tracer injections and two injections at the land surface, with detailed monitoring at several sampling sites inside the caves and at the spring (Figs. 1 and 2).

The study had five major goals: (1) localize and quantify the hydraulic connections between the two water caves and towards the karst spring; (2) reveal and characterize the supposed hierarchical drainage structure of the aquifer system; (3) delineate subcatchments within the large overall spring catchment area; (4) obtain spatially resolved information on flow velocities and transport parameters in the vadose, epiphreatic and phreatic zones; (5) estimate the water volume in the conduit network in comparison with results by Geyer et al. (2011).

2 Field site

The Blautopf ("Blue Pot") spring is located at the southern margin of the Swabian–Franconian Alb, Germany's largest karst area (Fig. 1). It drains an area of 165 km^2 and has a mean discharge of 2.3 $m^3\ s^{-1}$, with variation ranging from 0.3 $m^3\ s^{-1}$ in dry periods up to 32.5 $m^3\ s^{-1}$ during high flow conditions. The stratigraphy is composed of

a series of Upper Jurassic limestone and marl with a total thickness of up to 400 m. The aquifer system consists of an upper and lower karst aquifer, separated and underlain by marl aquitards (Bartenbach et al., 2009; Lauber et al., 2013). The landscape is characterized by numerous dolines and dry valleys. The lowering of the main valley during Plio–Pleistocene and the subsequent backfilling with gravel have created a deep karst system, i.e., the basis of the karst aquifer is below the level of the valley and main spring (Bartenbach and Ufrecht, 2009; Ufrecht, 2009). Waste water and agricultural sewage affect the water quality of the Blautopf karst spring that cannot be used for drinking water supply.

More than 150 caves have been mapped in the area (Arbeitsgemeinschaft Blautopf, 2011; Bohnert, 2009). The most important one is the Blauhöhlensystem ("Blue Cave System", southern cave in Figs. 1 and 2). Previously, the Blautopf spring was the only entrance to the systems. Cavers had to dive 1200 m to access and explore the inner parts of this cave. Since 2010, a drilled shaft allows direct access to the cave system without diving. The Blue Cave System is more than 10 km long and consist of phreatic (fully water-saturated), epiphreatic (open-channel flow) and dry passages (Fig. 2). Another important cave is the 3.5 km long Hessenhauhöhle ("Hessenhau Cave", northern cave). The entrance of the cave is a vertical shaft under a doline passing into a horizontal water cave in a depth of 130 m (Fig. 2). This cave was supposed to drain towards the Blue Cave System and Blautopf spring, but without clear evidence.

3 Methods

3.1 Tracer tests

The first two tracer injections into cave streams were done on 21 April 2012: 100 g of Uranine were injected in the northern cave at IP-1, and 200 g of Sulphorhodamine G (Sulpho G) were injected in the southern cave at IP-2 (Figs. 1 and 2). One week later, on 28 April 2012, two injections were done at the land surface, in distal parts of

the catchment area. It was possible to use the same two dye-tracers again, because monitoring in the active caves and at the spring has demonstrated that tracer concentrations from the first experiment had dropped below detection limit. 1500 g of Uranine were injected in a vertical karst shaft at IP-3 near the community of Laichingen, about 10 km away from the spring. For decades, this shaft had been used to dispose of overflow water from a sewage treatment plant. 2000 g of Sulpho G were injected in a doline at IP-4 in the village of Zainingen, 19 km away from the spring (Fig. 1). A minimum of 78 m^3 of water were used at each surface injection site to flush the tracer through the vadose zone.

In order to obtain detailed tracer breakthrough curves, three field fluorimeters (GGUN-FL 43, 334 und 335, Albillia, Switzerland) were installed at sampling points in the cave system (SP-2 and 3) and at the spring (SP-4) (Fig. 2). The fluorimeters were calibrated using water from the cave system. At SP-1, water samples were taken manually by cavers; water samples were also collected at other sites in order to check the fluorimeter results. Additionally, charcoal bags were installed at several sites in the cave system and replaced at least every two weeks. Water samples and charcoal bags were analysed in the KIT laboratory using a spectrofluorimeter (LS 55, Perkin Elmer).

In both cave systems (SP-1 and 2), discharge measurements were conducted one week before the tracer tests using the salt-dilution method. Discharge data from the spring were obtained from the regional authority.

3.2 Evaluation and modeling of the results

Flow velocities and dispersion/dispersivity were calculated with and without considering tortuosity. For this karst system, a tortuosity of 1.7 was obtained by dividing the surveyed length of the phreatic cave passage between SP-3 and the spring (1200 m) by the linear distance (700 m) (Fig. 1). For the sake of simplicity, all velocities and dispersions mentioned in the text are without considering tortuosity. Transit times and velocities between individual sampling points were calculated on the basis of peak transit times. By observing breakthrough curves (BTCs) at different parts in the cave

system (SP-2, SP-3) and at the spring (SP-4), it was possible to obtain flow parameters for individual epiphreatic and phreatic sections in the cave system (Fig. 2). Breakthrough curves were analytically modeled with a conventional advection dispersion model (ADM) and a two-region non-equilibrium (2RNE) model using the software CXTFIT (Toride et al., 1999). The 2RNE model accounts for exchange between mobile and immobile fluid regions in the karst system (Field and Pinsky, 2000).

Due to the nearly symmetric shapes of the breakthrough curves and the short tailing, most of the BTCs were fitted well with both models. As the 2RNE model may deliver multiple pairs of values, the ADM was used to obtain more robust values; results of the modeling (ADM) are listed in Table 1 and used for discussion. Mean square errors (RMSE) of all BTCs are greater than 0.931. Additional flow parameters for epiphreatic and phreatic zones, partitioning coefficient and mass transfer coefficient, were determined with the 2RNE model for selected BTCs of cave injections. Effects of the vadose zone were estimated by comparing parameters of surface and cave injections.

4 Results and discussion

4.1 Results of the tracer injections in cave streams

All observed BTCs resulting from the two injections in cave streams (IP-1 and IP-2) show a single and nearly symmetric peak and a short tailing (Fig. 3). Uranine (IP-1) was detected at SP-3 and at the spring (SP-4). The first detection occurred 26 h after injection. The maximum concentration of 1.9 $\mu g\,L^{-1}$ was reached after 32 h. At SP-4, Uranine was first detected after 41 h, and the maximum of 1.1 $\mu g\,L^{-1}$ occurred after 49 h. Spring discharge was about 1.24 $m^3\,s^{-1}$. Despite direct injection in the cave stream, total tracer recovery only reached 52 % (Table 1). Mean flow velocities of 74 $m\,h^{-1}$ and a dispersion of 734 $m^2\,h^{-1}$ were calculated between IP-1 and SP-3 (without considering tortuosity). Between IP-1 and SP-4, mean flow velocities were lower with 64 $m\,h^{-1}$; dispersion was 784 $m^2\,h^{-1}$. The flow velocities in the phreatic sections between SP-3

and SP-4 are about 41 $m\,h^{-1}$. Uranine was not detected at SP-2, in the more distant and upstream part of the southern cave.

Sulpho G (IP-2) was detected at all three sampling points, SP-2, SP-3 and SP-4, tracing the flowpath through the southern cave. The first arrival at SP-2 occurred 1 h after injection; the maximum of 50 $\mu g\,L^{-1}$ was reached after 2 h 15 min (Fig. 3). At SP-3, first detection was after 12 h, maximum concentration of 6 $\mu g\,L^{-1}$ was measured after 16 h. Sulpho G arrived after 25 h at the spring where the maximum of 4.0 $\mu g\,L^{-1}$ occurred after 30 h. During breakthrough, spring discharge was 1.32 $m^3\,s^{-1}$, and 79 % of the tracer were recovered (Table 1). Highest mean flow velocities, 275 $m\,h^{-1}$, were calculated for the epiphreatic section between IP-2 and SP-2; dispersion is 4920 $m^2\,h^{-1}$. Significantly lower values for mean flow velocity (112 $m\,h^{-1}$) and dispersion (1160 $m\,h^{-1}$) were found between IP-2 and SP-3. The lowest flow velocities, 47 $m\,h^{-1}$, were measured in the phreatic section between SP-3 and the spring. After 75 h, concentrations at the spring had decreased below detection limit (Fig. 3).

4.2 Results of the tracer injections at the land surface

Uranine (IP-3) was detected at SP-1, SP-3 and the spring (SP-4) (Fig. 4). Due to the poor accessibility of the northern cave, sampling at SP-1 was only temporarily feasible and the BTC is thus incomplete. Uranine was first detected at SP-1 after 98 h. The first arrival at SP-3 occurred after 136 h, and the maximum of 11.5 $\mu g\,L^{-1}$ was reached after 155 h. At SP-4, first detection was after 153 h and maximum concentration of 10.3 $\mu g\,L^{-1}$ was measured after 181 h. Despite the injection via the unsaturated zone (into a karst shaft), the BTCs display a single peak and nearly symmetric shapes. During breakthrough, spring discharge was about 1.04 $m^3\,s^{-1}$, and a recovery of 63 % was calculated (Table 1). Maximum flow velocity between IP-3 and SP-1 is 69 $m\,h^{-1}$. Mean flow velocity from IP-3 to SP-3 was calculated with 56 $m\,h^{-1}$, dispersion is 794 $m^2\,h^{-1}$. Approaching the spring, mean flow velocities decline to 56 $m\,h^{-1}$ and dispersion decreases slightly to 727 $m^2\,h^{-1}$.

Sulpho G from IP-4 was only detected in the southern cave. All BTCs at SP-2, SP-3 and the spring (SP-4) display two peaks with maximum concentrations between 0.1 and 0.7 µg L^{-1} (Fig. 4). First detection at SP-4 was 357 h after injection, the first tracer maximum occurred after 405 h with 0.14 µg L^{-1}. Mean spring discharge was 0.97 m^3 s^{-1} and only 5 % of this tracer was recovered. The results indicate that sorption processes in the vadose zone and remobilization after a rain event have caused the second peak. Due to rainfall, spring discharge increased up to 1.25 m^3 s^{-1}between the two peaks, causing dilution of the tracer. Maximum flow velocity from IP-4 to SP-4 is 53 m h^{-1}, mean flow velocity for the first peak is 45 m h^{-1}. The existence of two separate flowpaths can be largely ruled out, as a previous tracer test at the same injection site in 1986 exhibits a breakthrough with a single peak. Spring discharge had been about 3.20 m^3 s^{-1} and recovery about 90 % (Villinger and Ufrecht, 1989). Therefore, only the first peak of the BTC of this injection is modeled with CXTFIT.

4.3 Structure of the drainage network

Uranine BTCs from injections IP-1 and IP-3 monitored at SP-3 demonstrate that there is connection between the two caves (Figs. 2–4). Uranine was also detected at the spring (SP-4), but not in upstream parts of the southern cave (SP-2). The high similarity and the single-peaked shapes of the BTCs observed at SP-3 and SP-4 suggest that there is only one flowpath connecting the two caves. Results from charcoal bags make it possible to further constrain the location of the connecting conduit – this is valuable information for the further exploration of the cave.

Two main branches of drainage have been developed with approximation to the spring – the two known caves (Figs. 2 and 5). This is confirmed by discharge measurements, conducted in both cave systems. In the northern cave, a channel flow of 0.77 m^3 s^{-1} was determined, while a flow of about 0.69 m^3 s^{-1} was measured at SP-2 in the southern cave. At that time, discharge at the spring was 1.30 m^3 s^{-1}. Therewith, both cave streams contribute approximately 50 % to the whole discharge of the spring.

Based on continuous tracer monitoring in the caves, it was possible to subdivide the catchment area of the Blautopf karst spring into two sub-catchments contributing to the two active water caves (Fig. 5). The northeastern part of the area drains via the northern cave to the spring, while the southwestern sub-catchment is connected to the southern cave (IP-2). In a distance of 700 m to the spring, the two cave streams confluence just ahead of SP-3 and form a single, large phreatic cave passage towards the main outlet. Similar drainage structures are known from numerical models (e.g. Worthington and Ford, 2009) and proven by using tracer tests in the catchment area of Milandre cave (Perrin et al., 2007) and Mammoth cave system (Meiman et al., 2001).

4.4 Flow velocities and flow parameters in the karst system

Whereas conventional tracer tests with injections at the surface and monitoring at the spring represent mixed information from the entire flowpath, the tracer tests presented in this study made it possible to differentiate flow in vadose, epiphreatic and phreatic cave sections. In the two cave systems, clear relations between flow types, hydraulic gradients and flow velocities have been found. The highest (mean) flow velocities of 275 m h^{-1} were found in the epiphreatic passage between IP-2 and SP-2. Considering a tortuosity of 1.7, maximum mean flow velocities may reach 468 m h^{-1}. The hydraulic gradient is highest in this section with about 40 ‰ (Fig. 6). Flow velocities decrease with approximation to the main outlet as the hydraulic gradient decreases. Until SP-3, flow velocities decrease down to 84 m h^{-1} at a gradient of 2 ‰. The different hydraulic gradients can be related to different stages of cave development. Lowest flow velocities of 26 to 47 m h^{-1} were found in the phreatic cave passage between SP-3 and the spring. There, conduit cross-sections (A) become very large and result in a decrease of flow velocities (v) according to the condition of flow continuity ($Q = vA$). Additionally, large phreatic conduits lead on to a high conductivity and therewith a very low hydraulic gradient. This gives rise to impoundment in the phreatic zone and the formation of underground lakes in the nearby epiphreatic cave passages. As observed at the phreatic cave passage, flow velocities also vary with flow conditions during all four tracer tests.

Discharge fluctuated between 0.97 to 1.32 $m^3 s^{-1}$, while flow velocities varied between 21 $m h^{-1}$ during lower flow conditions and 47 $m h^{-1}$ during higher flow conditions.

Spatially, dispersion coefficients vary with flow velocities. Highest values for dispersion were calculated for remote parts of the cave system with 4920 $m^2 h^{-1}$ (Fig. 6). There, cascades, waterfalls and rapids cause very high dispersion (Hauns et al., 2001). However, with approximation to the spring, low hydraulic gradients and low flow velocities result in a lower dispersion of about 734–1160 $m^2 h^{-1}$ for in-cave injections (IP-1, IP-2). A decrease of dispersion and flow velocities in approximation to the spring were also made in a cave system in Slovenia (Gabrovsek et al., 2010).

The strongly karstified vadose zone at IP-3 reveals little hydraulic impact on groundwater flow. Maximum flow velocities of 69 $m h^{-1}$ were found for the flow through vadose and epiphreatic zone from IP-3 to SP-1, whereas maximum flow velocities of 68–96 $m h^{-1}$ were found for the following cave passage between SP-1 and SP-3 (IP-1, IP-3, Table 1, Fig. 7). The BTCs of injections IP-1 and IP-3 are both exhibiting a symmetric peak and a short tailing, no essential difference between cave and surface injection has been observed. The minor influence of the vadose zone may be provoked by injections in highly karstified zones, e.g. karst shafts and dolines. But also may be a scale effect: the thickness of the vadose zone is about 100 m and therewith insignificant in respect to the whole flow path of at least 10 000 m. However, water must flow two times through a marly formation to reach the spring which has previously assumed to have a low permeability. Low flow velocities were found for IP-4, but can be reduced to low flow conditions during the tracer test (Fig. 6).

Dispersion coefficients of in-cave and surface injections are partly different. Results from IP-3 exhibit a low dispersion of 727 $m^2 h^{-1}$, which is similar to in-cave values (IP-3, Fig. 7). However, geologic profiles show that the karst water lies within the lower karst aquifer and flow paths must cross the marly formation twice to drain to the spring (Lauber et al., 2013). Despite that, dispersion does not increase significantly, indicating a high permeability in the vadose zone. In contrast to this, values observed from IP-4 show significant higher values of 3260 to 16 700 $m^2 h^{-1}$ fitting to the predominating

circumstances: long flow distances and flow through unsaturated zone. These results are related to analysis of the first peak and therefore may have uncertainties.

To eliminate the influence of flow velocity, the dispersivity ($\alpha = D/v$) was calculated for all measuring points. Most values lie within 10–18 m (IP-1 to IP-3). There is apparently no significant increase with flow distance within the active cave system. In contrary, the reverse was observed for IP-2: dispersivity decreases with increasing flow distance (Fig. 6). This may be reduced to flow in large channels with few turbulences and heterogeneities. Similar effects have been observed by Gabrovsek et al. (2010) in a cave system in Slovenia. However, Hauns et al. (2001) found a strong correlation of dispersivity and flow distance in a cave system in Switzerland. An increase of dispersivity has also been observed by numerous previous surface tracer tests in this catchment area of Blautopf (Villinger and Ufrecht, 1989). Values from 12.4 to 38.1 m have been determined for distances between 3.7 and 19.0 km. The low values of the cave system (IP-1 and IP-2) fit well to these dispersivity values. It seems that flow through unsaturated zone may reveal two diverse effects on dispersivity; only little increase of dispersivity (IP-3) probably due to extreme karstified zones and a major influence (IP-4) due to less karstified zones.

Model results with 2RNE-model of CXTFIT show a high percentage of karst water flowing in the mobile phase (89–97 %). This was calculated for cave and surface injections, showing highly karstified and permeable flow paths. The mean value of mass transfer coefficient from in-cave injections is 0.62 demonstrating low mass transfer between immobile and mobile phase in epiphreatic and phreatic zones, whereas higher mean value from surface injections (about 1.2) indicate a higher mass transfer, probably present in the vadose zone.

Large areas of the catchment area are dominated by diffuse infiltration. By using water balances, spring hydrograph analysis and natural tracers the water volume in the fractured matrix was estimated with 90 to 95 % of the total karst water (Geyer et al., 2011; Bauer and Selg, 2006; Schwarz et al., 2009; Selg and Schwarz, 2009), the total water volume was denoted with 27 Mm^3. The mean residence time was calculated with

up to 15 yr. During the tracer tests of this study, a water volume of 0.68 resp. 1.42 Mm^3 was calculated for each sub-catchment area (IP-3 resp. IP-4). The water volume in the phreatic conduit between the confluence of the sub-catchment streams and the spring is about 0.08 Mm^3. The total water volume of the conduit water is about 2.0 Mm^3 during low flow conditions at 1 $m^3 s^{-1}$ and therewith corresponds to a fraction of about 7 % of the total karst water of 27 Mm^3.

5 Conclusions

The results of the in-cave dye-tracing and monitoring enabled detailed knowledge of the internal drainage structure and hydraulic properties. It was possible to demonstrate that there is exactly one hydraulic connection between both caves; the confluence is located about 700 m (linear distance) upstream of the spring. In combination with land surface injections and in-cave monitoring the dendritic drainage structure of the karst system was proven for the first time. Within the whole catchment area of the spring two sub-catchment areas were identified, drained by an active karst conduit contributing to about 50 % to the discharge of the spring. The northeastern sub-catchment drains via the northern cave, whereas the southwestern sub-catchment is linked with the southern cave. In a distance of approximately 700 m to the spring, both main drainage conduits converge and form one big phreatic cave passage.

For the first time high resolved information about flow velocities and transport parameters were obtained for single cave passages. Flow velocities vary strongly within the cave systems; highest flow velocities are coupled with high hydraulic gradient and found in epiphreatic cave passages. Significant lower flow velocities were determined for the phreatic cave passage, showing a very low hydraulic gradient and large conduit cross-sections. This leads to impoundment of water in these parts of the cave system. Dispersion is highly variable due to flow velocities. Highest dispersion was attested for epiphreatic conduits with high flow velocity in remote parts of the cave system, whereas low dispersion exists generally in conduits with low flow velocities close to the spring.

Dispersivity displays relatively constant values and does not significantly increase with increasing flow path, reflecting a strong karstification. With approximation to the spring, large conduits with less turbulences and heterogeneities influence flow parameters.

Water volume of the conduit system was estimated and correlates with values from water balances and spring hydrograph analysis. During low flow conditions, the fraction of conduit water is about 7 % of the total karst water. Due to rural and agricultural land-use, the water quality of the Blautopf is affected. The obtained parameters and spatially high resolved information allows a better understanding of the structure of the karst system and may help to protect and preserve karst water resources.

Acknowledgements. We thank all cavers of the caving associations Arge Blautopf and Arge Blaukarst for the excellent cooperation, allocation of cave maps and support during the tracer tests in the two caves, especially Andreas Kücha and Jürgen Bohnert. Financial support was given by the Stuttgarter Hofbräu Environmental Foundation. We acknowledge support by Deutsche Forschungsgemeinschaft and Open Access Publishing Fund of Karlsruhe Institute of Technology.

The service charges for this open access publication
have been covered by a Research Centre of the
Helmholtz Association.

References

Arbeitsgemeinschaft Blautopf: Faszination Blautopf – Vorstoß in unbekannte Höhlenwelten, Jan Thorbecke, Ostfildern, 2011.

Armbuster, V. and Selg, M.: Der Abfluss des Blautopfs im Spiegel der Grundwasserneubildung (Oberjura–Karst, Süddeutschland), Tübinger Geowissenschaftliche Arbeiten, C 98, 1–16, 2006.

Bartenbach, M. and Ufrecht, W.: Stratigraphie und Fazies des Oberjuras im Umfeld der Blaubeurer Talschlinge – Ergebnisse einer Bohrung und Untertagekartierung im Blauhöhlensystem, Laichinger Höhlenfreund, 44, 89–106, 2009.

Bartenbach, M., Möbius, R., and Aigner, T.: Neue Daten zur Geologie (Schichtenfolge, Fazies) des Oberjuras im Einzugsgebiet des Blautopfs, Laichinger Höhlenfreund, 44, 73–88, 2009.
Bauer, M. and Selg, M.: Altersstruktur und mittlere Verweilzeit im Grundwasser des Blautopfs und anderer Quellen und Brunnen im Oberjura–Karst Süddeutschlands, Tübinger Geowissenschaftliche Arbeiten (TGA), C 98, 17–44, 2006.
Bohnert, J.: Zum Stand der speläologischen Erforschung von Hessenhauhöhle (7524/117) und Seligengrundhöhle (7524/119) durch die Arbeitsgemeinschaft Blaukarst, Laichinger Höhlenfreund, 44, 37–44, 2009.
Dreybrodt, W., Romanov, D., and Kaufmann, G.: Evolution of caves in porous limestone by mixing corrosion: a model approach, Geol. Croat., 63, 129–135, 2010.
Field, M. S. and Pinsky, P. F.: A two-region nonequilibrium model for solute transport in solution conduits in karstic aquifers, J. Contam. Hydrol., 44, 329–351, 2000.
Gabrovsek, F., Romanov, D., and Dreybrodt, W.: Early karstification in a dual-fracture aquifer: the role of exchange flow between prominent fractures and a dense net of fissures, J. Hydrol., 299, 45–66, 2004.
Gabrovsek, F., Kogovsek, J., Kovacic, G., Petric, M., Ravbar, N., and Turk, J.: Recent results of tracer tests in the catchment of the Unica River (SW Slovenia), Acta Carsologica, 39, 27–37, 2010.
Geyer, T., Birk, S., Licha, T., Liedl, R., and Sauter, M.: Multitracer test approach to characterize reactive transport in karst aquifers, Ground Water, 45, 36–45, 2007.
Geyer, T., Selg, M., Gudera, T., and Sauter, M.: Langzeitabflussverhalten der Gallusquelle und des Blautopfs – relative Bedeutung der Matrix und des Großkluftsystems, Laichinger Höhlenfreund, 46, 63–74, 2011.
Goldscheider, N., Meiman, J., Pronk, M., and Smart, C.: Tracer tests in karst hydrogeology and speleology, Int. J. Speleol., 37, 27–40, 2008.
Göppert, N. and Goldscheider, N.: Solute and colloid transport in karst conduits under low- and high-flow conditions, Ground Water, 46, 61–68, 2008.
Hauns, M., Jeannin, P.-Y., and Atteia, O.: Dispersion, retardation and scale effect in tracer breakthrough curves in karst conduits, J. Hydrol., 241, 177–193, 2001.
Lauber, U., Ufrecht, W., and Goldscheider, N.: Neue Erkenntnisse zur Struktur der Karstentwässerung im aktiven Höhlensystem des Blautopfs, Grundwasser, accepted, 2013.

Massei, N., Wang, H. Q., Field, M. S., Dupont, J. P., Bakalowicz, M., and Rodet, J.: Interpreting tracer breakthrough tailing in a conduit-dominated karstic aquifer, Hydrogeol. J., 14, 849–858, 2006.
Meiman, J., Groves, C., and Herstein, S.: In-cave dye tracing and drainage basin divides in the Mammoth Cave karst aquifer, Kentucky, US Geological Survey, Water Resources Investigations Report, 01–4011, 179–185, 2001.
Morales, T., Valderrama, I., Uriarte, J., Antigüedad, I., and Olazar, M.: Predicting travel times and transport characterization in karst conduits by analyzing tracer-breakthrough curves, J. Hydrol., 334, 183–198, 2007.
Palmer, A. N.: Origin and morphology of limestone caves, Geol. Soc. Am. Bull., 103, 1–21, 1991.
Perrin, J., Jeannin, P.-Y., and Cornaton, F.: The role of tributary mixing in chemical variations at a karst spring, Milandre, Switzerland, J. Hydrol., 322, 158–173, 2007.
Pronk, M., Goldscheider, N., Zopfi, J., and Zwahlen, F.: Percolation and particle transport in the unsaturated zone of a karst aquifer, Ground Water, 47, 361–369, 2009.
Schwarz, K., Barth, J. A. C., Postigo-Rebollo, C., and Grathwohl, P.: Mixing and transport of water in a karst catchment: a case study from precipitation via seepage to the spring, Hydrol. Earth Syst. Sci., 13, 285–292, doi:10.5194/hess-13-285-2009, 2009.
Selg, M. and Schwarz, K.: Am Puls der schönen Lau – zur Hydrogeologie des Blautopf-Einzugsgebietes, Laichinger Höhlenfreund, 44, 45–72, 2009.
Smart, C. C.: Artificial tracer techniques for the determination of the structure of conduit aquifers, Ground Water, 26, 445–453, 1988.
Toride, N., Leij, F. J., and van Genuchten, M. T.: The CXTFIT code for estimating transport parameters from laboratory or field tracer experiments, ARS Research Report No. 137, US Salinity Laboratory USDA, Riverside, California, 1999.
Ufrecht, W.: Schichtlagerung und Bruchtektonik im Einzugsgebiet des Blautopfs und dessen Umfeld (Mittlere Schwäbische Alb), Laichinger Höhlenfreund, 44, 107–148, 2009.
Villinger, E. and Ufrecht, W.: Ergebnisse neuer Markierungsversuche im Einzugsgebiet des Blautopfs (mittlere Schwäbische Alb), Mitt. Verb. dt. Höhlen- u. Karstforscher, 35, 25–38, 1989.

Table 1. Results of the tracer test.

Injection / Sampling	Injection Points / Tracer / Type of Injection Point		IP-1 Uranine Cave stream	IP-2 Sulpho G Cave stream	IP-3 Uranine Karst shaft	IP-4 Sulpho G Doline
Sampling Points	Parameter	Unit				
SP-1	Time of first detection[a]	h	= injection point	no detection	98.1	no detection
	Maximum velocity[a]	$m\,h^{-1}$			69/118	
SP-2	Time of first detection	h	no detection	1.2	no detection	320
	Peak time	h		2.3		360
	Maximum concentration	$\mu g\,L^{-1}$		50.7		0.6
	Maximum velocity	$m\,h^{-1}$		578/983		51/87
	Peak velocity	$m\,h^{-1}$		290/493		45/77
	Mean flow velocity	$m\,h^{-1}$		275/468		–
	Dispersion	$m^2\,h^{-1}$		4920/14 200		–
	Dispersivity	m		18/30		–
SP-3	Time of first detection	h	26.0	12.0	136.0	335
	Peak time	h	31.8	15.9	154.6	385
	Maximum concentration	$\mu g\,L^{-1}$	1.9	6.0	11.5	0.5
	Maximum velocity	$m\,h^{-1}$	96/163	152/258	68/115	54/91
	Peak velocity	$m\,h^{-1}$	78/132	115/195	60/102	46/79
	Mean flow velocity	$m\,h^{-1}$	74/130	112/191	56/100	45/74[b]
	Dispersion	$m^2\,h^{-1}$	734/2350	1160/3360	794/2290	6230/16 700[b]
	Dispersivity	m	10/18	10/17	14.2/22.9	138/225[b]
SP-4	Time of first detection	h	41.0	25.6	153	357
	Peak time	h	48.8	29.2	180.9	405
	Maximum concentration	$\mu g\,L^{-1}$	1.1	4.0	10.3	0.14
	Distance to spring	km	3.2/5.4	2.5/4.3	10/17	19/32
	Maximum velocity	$m\,h^{-1}$	78/132	98/167	65/111	53/91
	Peak velocity	$m\,h^{-1}$	65/111	86/147	55/94	46/80
	Spring discharge	$m^3\,s^{-1}$	1.24	1.32	1.04	0.97
	Recovery	%	52	79	63	5
	Mean flow velocity	$m\,h^{-1}$	64/110	74/133	56/95	45/76[b]
	Dispersion	$m^2\,h^{-1}$	784/2270	1120/3300	727/2100	3260/9240[b]
	Dispersivity	m	12/20	15/25	12/22	74/121[b]
	Partitioning coefficient β	–	0.96	0.89	0.97	0.91[b]
	Mass transfer coefficient ω	–	0.57	0.82	0.39	1.37[b]

Note: mean flow velocity and dispersion are calculated by using ADM of the program CXTFIT (Toride et al., 1999). Coefficients of determinations are greater than 0.931. First values are determined without/with respect to tortuosity. Partitioning coefficients and mass transfer coefficients are calculated by using 2RNE-model of CXTFIT.
[a] incomplete BTC.
[b] parameters are only calculated for the first peak, coefficients of determinations are greater than 0.800.

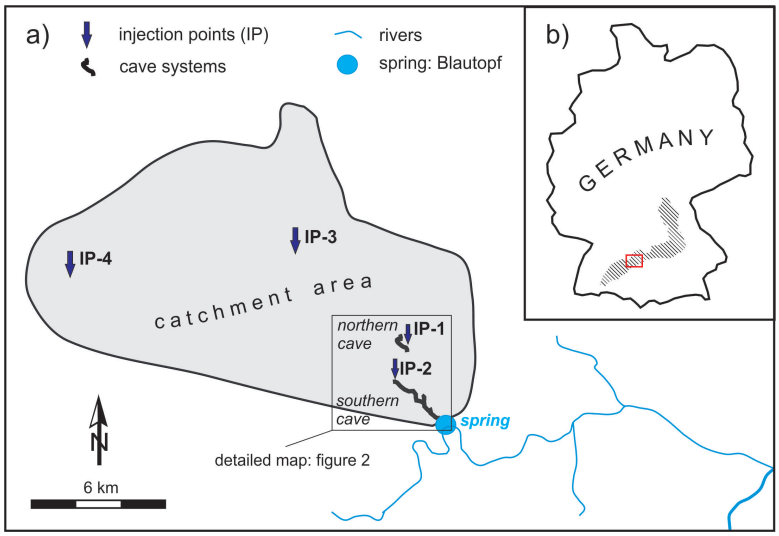

Fig. 1. (a) Catchment area of the Blautopf spring with location of the Blue Cave System (southern cave), the Hessenhau Cave (northern cave) and the four tracer injection sites; **(b)** location of the test site (rectangle) within the South German karst region of the Swabian and Franconian Alb (shaded).

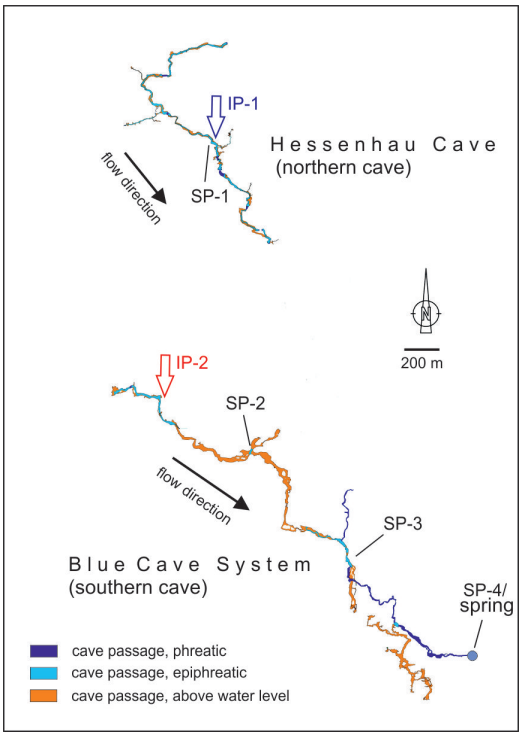

Fig. 2. Map of the two caves with indication of phreatic, epiphreatic and dry cave passages, injection points IP-1 and IP-2 in the cave streams and sampling points (SP-1 to SP-4); mapping of caves by Arge Blautopf and Arge Blaukarst.

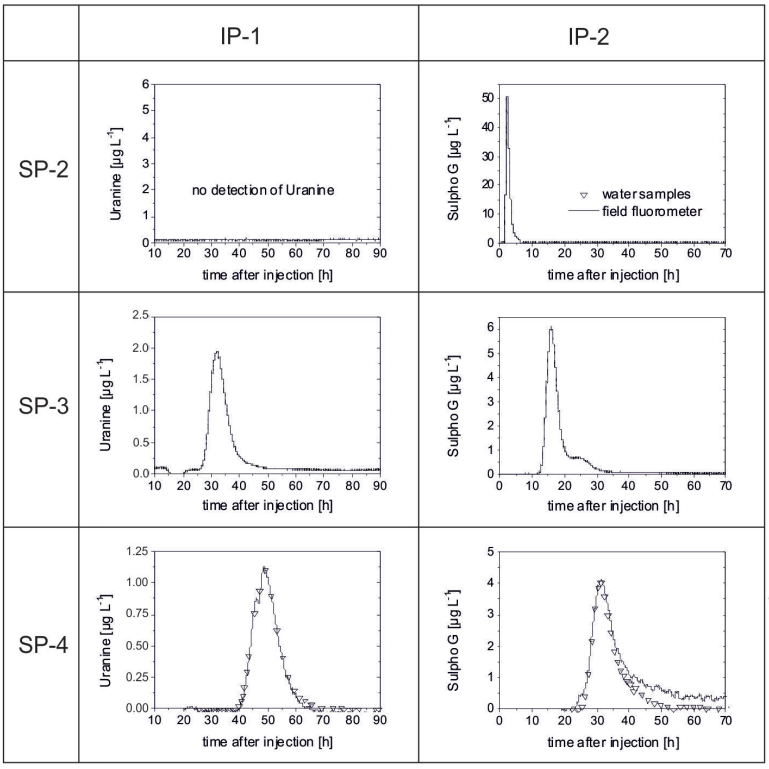

Fig. 3. Breakthrough curves resulting from in-cave dye-tracer injection at IP-1 (Uranine) and IP-2 (Sulpho G) obtained at sampling points in the cave (SP-2, SP-3) and at the spring (SP-4).

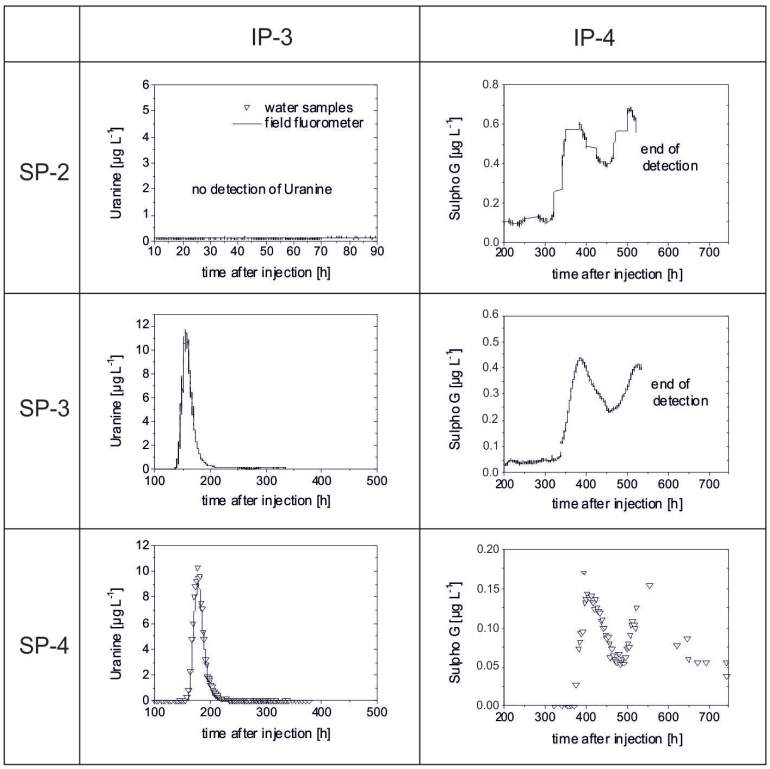

Fig. 4. Breakthrough curves resulting from injections at the land surface, at IP-3 (Uranine) and IP-4 (Sulpho G), observed at sampling points in the cave (SP-2, SP-3) and at the spring (SP-4).

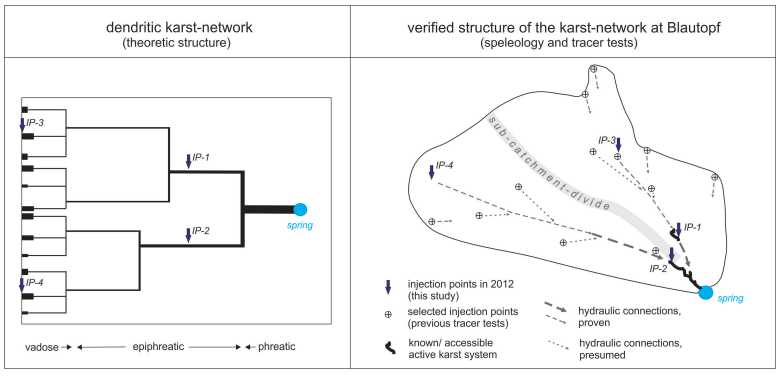

Fig. 5. Theoretic structure of a hierarchical karst network, and verified structure of the Blautopf spring catchment area that consists of two sub-catchments draining towards the northern and southern cave, respectively. The caves converge about 700 m linear distance upstream of the spring.

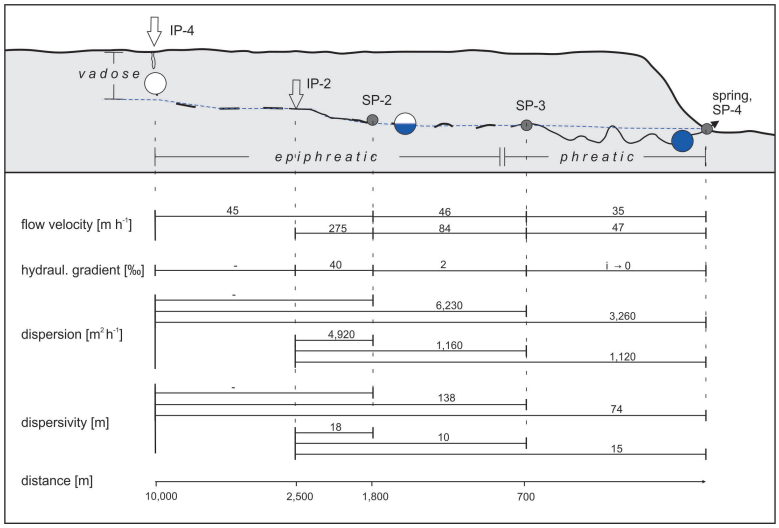

Fig. 6. Schematic sketch of injection and sampling points of the two tracer tests in the southern drainage system (Blue Cave System) with determined flow and transport parameters.

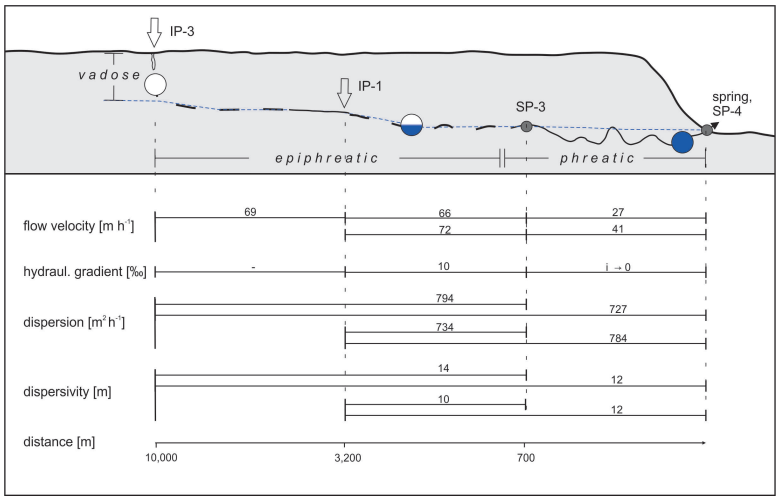

Fig. 7. Schematic sketch of the two tracer tests in the northern drainage system (Hessenhau Cave) with determined flow and transport parameters.

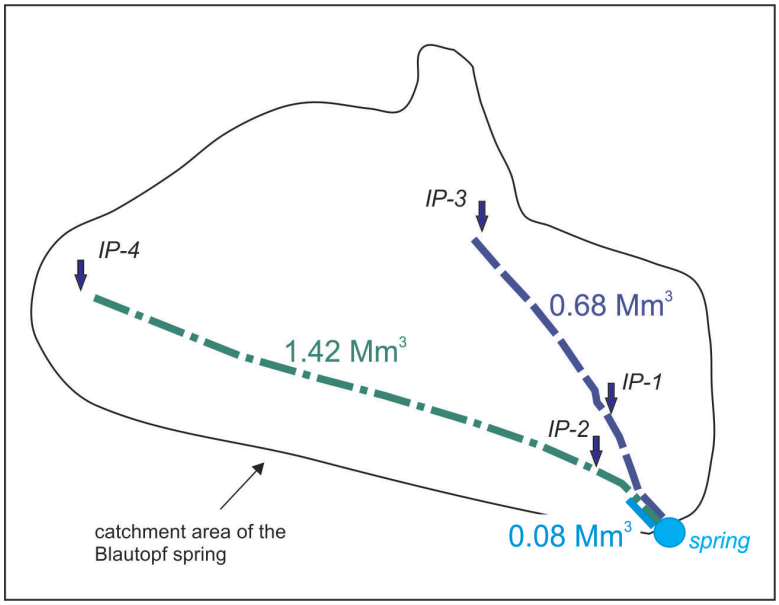

Fig. 8. Conduit water volumes estimated for each drainage system and the phreatic cave passage on the basis of the tracer test results. The total conduit volume is about 2.0 Mm^3.